Remote Sensing Letters
Vol. 1, No. 2, June 2010, 95–102

Taylor & Francis
Taylor & Francis Group

Replacing pixel representations by point-function schemes for reducing discretization error in ill-posed remote sensing problems, with examples from cloud tomography

DONG HUANG*, YANGANG LIU and WARREN WISCOMBE
Environmental Sciences Department, Brookhaven National Laboratory, Upton, NY 11973, USA

(*Received 29 April 2009; in final form 23 June 2009*)

Because of their simplicity and low computational cost, discretizations based on pixels have held sway in remote sensing since its inception. Yet functional representations are clearly superior in many applications, for example when combining retrievals from dissimilar remote sensing instruments. Using cloud tomography as an example, this letter shows that a point-function discretization scheme based on linear interpolation can reduce retrieval error of cloud water content up to 40% compared to a conventional pixel scheme. This improvement is particularly marked because cloud tomography, like the vast majority of remote sensing problems, is ill-posed and thus a small inaccuracy in the formulation of the retrieval problem, such as discretization error, can cause a large error in the retrievals.

1. Introduction

Discretizations based on pixels have held sway in remote sensing since its inception. These pixel discretization schemes have shown many disadvantages as earth observations are relying more and more on multi-sensor data. For example, the NASA EOS A-train satellites carrying many dissimilar sensors (active vs. passive, different instantaneous field of view, etc.) have provided unprecedented data for comprehensive studies of Earth's weather and climate (Stephens *et al.* 2002). In the pixel framework, the mismatch of pixel sizes used in various satellite products poses many challenges for data integration. The pixel scheme can also introduce artefacts in ground-based remote sensing. The beam of a ground microwave radiometer, for example, is a cone extended from the radiometer and the actual width of the beam varies with height; this cone is not naturally matched by rectangular pixels.

Furthermore, the inverse problems of remote sensing are often ill-posed, making the retrieval sensitive to small inaccuracies such as discretization errors. Discretization errors will be magnified in numerical inversion procedures, making the retrieval even more inaccurate (Bockmann 2001). Superficially, it would seem that discretization error could be reduced by using smaller grids/pixels, but in practice this may not improve the retrieval. This is because finer grids lead to a larger number of unknowns, thus a higher dimension in the inverse problem, which in turn makes the inverse problem more ill-posed and thus the retrieval more sensitive to perturbations (Hansen 1998). The trade-off between discretization and ill-posedness limits the ability of remote sensing to resolve

*Corresponding author. Email: dhuang@bnl.gov

Remote Sensing Letters
ISSN 2150-704X print/ISSN 2150-7058 online
http://www.tandf.co.uk/journals
DOI: 10.1080/01431160903140779

the desired variables at fine spatial scales. The interweaving issue of ill-posing and discretization needs to be addressed to improve the remote sensing retrievals.

Functional representation was initially proposed for medical image reconstruction problems as an alternative to transform methods (Censor 1983). The functional approach has also been found to be valuable for remote sensing problems like infrared sounding of atmospheric temperature and constituent profiles (Susskind *et al.* 2003). With a functional representation satellite images can be resampled at any resolution and thus can help the problem of resolution mismatch between different satellite products, although the minimal resolvable scale, of course, is limited by the inherent resolution of the instrument. For inverse retrieval problems, functional representations can further help the interweaving issue of ill-posedness and discretization error. The variable to be retrieved is expressed as a superposition of some prescribed basis functions, usually orthogonal empirical functions derived from historical observations or functions such as the Fourier basis and polynomials. Then the only unknowns are the coefficients for each basis function; in this way the discretization error can be reduced without increasing the dimension of the retrieval problem.

The objective of this research letter is to adopt a functional discretization scheme, called point-function discretization, through which a two-dimensional or three-dimensional (2D/3D) continuous field is approximated by interpolating a set of point values over the whole domain. Microwave cloud tomography is then used as an example to show that the point-function discretization scheme can be integrated into an inversion algorithm to reduce the discretization error and thus to improve the retrieval.

2. Pixel and point-function representations

Remote sensing retrieval problems can generally be formulated as *deriving the distribution of some desired variable* $x(r)$ *within a domain* Ω *from the set of remote sensing measurements* $\{b_i\}$. In many applications, the problem can be reduced to solving a set of Fredholm integral equations of the first kind (Arfken 1985):

$$\int_{r\in\Omega} a_i(r)x(r)\mathrm{d}r = b_i, \tag{1}$$

where $a_i(r)$ is a kernel function representing the forward operator that relates the desired variable $x(r)$ to the measurements $\{b_i\}$.

The spatial domain Ω can be partitioned into a multiplicity of overlapping or non-overlapping elements. Using overlapping elements inherently imposes a certain degree of smoothness in the retrieval, which can be an advantage for ill-posed inverse problems. Here, for simplicity, N non-overlapping elements E_i are chosen such that $U_{i=1}^{N} E_i \equiv \Omega$. The elements join at n vertex nodes e^j, $j = 1, \ldots, n$ (a node is a point at which three or more elements intersect). For simplicity, throughout this study equal-sized square elements are used so that the nodes are equally spaced by a distance d. The solution $x(r)$ to equation (1) is approximated by a superposition of a set of predefined basis functions $w(r, e^j)$:

$$x(r) \approx \sum_{j=1}^{n} w(r, e^j)x(e^j). \tag{2}$$

The inverse problem now is to find the nodal values $x(e^j)$ from which the solution everywhere in the domain Ω can be derived by the interpolation rule (2).

Unfortunately, in many applications the historical observations needed to empirically specify the basis functions are unavailable and one has to choose arbitrary bases. Different choices of the basis functions lead to different discretization models. This is illustrated as follows. Let e^j be the nearest node to an arbitrary location r. Setting the basis to the Kronecker delta function, i.e. $w(r, e^i) = w(e^j, e^i) = \delta_{ij}$, assures that $x(r)$ takes the same value in the box of size d centred at e^j. Hence the choice of the Kronecker delta function coincides with the conventional pixel scheme.

If the Kronecker delta bases are replaced with pyramidal-shaped basis functions, a new discretization scheme is obtained (Giuli *et al.* 1991). This is called the point-function discretization scheme here. Let (r_x, r_y) and (e^i_x, e^i_y) denote the coordinates of point r and node e^i in the 2D case and let the basis function be the bi-linear interpolation function:

$$w(r, e^i) \equiv (1 - t)(1 - u), \tag{3}$$

where $e^i_x \le r_x \le e^i_x + d$ and $e^i_y \le r_y \le e^i_y + d$, and $t \equiv (r_x - e^i_x)/d$, $u \equiv (r_y - e^i_y)/d$.

With the basis functions specified by equation (3), substituting equation (2) in equation (1) leads to

$$\sum_{j=1}^{n} x(e^j) \int_{r\in\Omega} a_i(r) w(r, e^j) \mathrm{d}r = b_i \tag{4}$$

Rewrite equation (4) as a matrix equation:

$$\mathbf{A}\boldsymbol{x} = \boldsymbol{b}, \tag{5}$$

where $\mathbf{A} \equiv (a_{ij})$ is an $m \times n$ kernel matrix representing the forward operator with its entry $a_{ij} = \int_{r\in\Omega} a_i(r) w(r, e^j) \mathrm{d}r$, $\boldsymbol{x}$ is the vector of desired variables at the n nodes, and $\boldsymbol{b}$ is the vector of remote sensing measurements. In this way, the retrieval problem is now reduced to solving the matrix equation (5) for a set of point values and then interpolating the point values to obtain the desired variables in the entire domain.

3. Application to microwave cloud tomography

Having concentrated on the mathematical description of the point-function discretization scheme, the next step is to apply this scheme to a practical remote sensing problem to examine its impacts on the retrieval accuracy.

3.1 *Cloud tomography and constrained inversion algorithm*

Cloud tomography is a method for retrieving 2D/3D fields of cloud liquid water content (LWC) from cloud thermal emission measurements (Warner *et al.* 1985). This method involves measuring the microwave cloud emission from a multiplicity of different directions by a single airborne or multiple ground-based radiometers and inverting the resulting radiometric data for the LWC field by numerical procedures. The tomographic retrieval problem is highly ill-posed especially when only a few ground-based radiometers are used, as shown in Huang *et al.* (2008a).

The conventional pixel scheme can produce artefacts in the tomographic retrievals (Scales *et al.* 1990; Delprat-Jannaud and Lailly 1993). As illustrated in figure 1, the sampling volume of each radiometer is mainly within a cone whose apex angle is

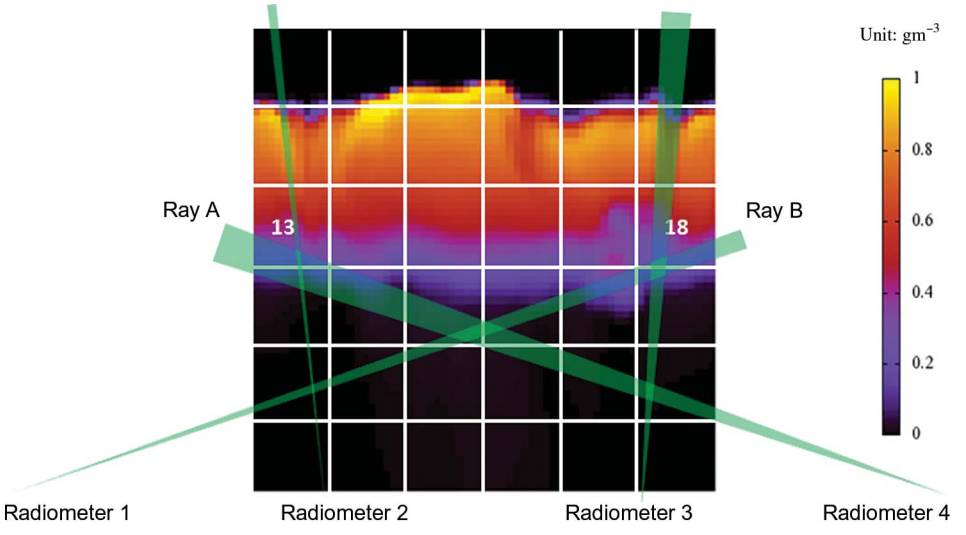

Figure 1. Discretization artefacts of the pixel scheme when using four ground radiometers of different antenna beam widths. Four microwave radiometers are equally spaced along a 10 km line. The 5 km wide 1.5 km high domain, divided into 6×6 pixels, contains a stratocumulus cloud. Note that some rays intersect a pixel through its corner, e.g. ray A in pixel 13. The brightness temperature measured along A is close to that of a clear sky. The resulting tomographic retrieval would yield very little liquid water in pixels 13 and 18, which is apparently not true.

determined by the antenna beam width. It is thus not surprising that dividing the retrieval space into rectangular boxes will introduce artefacts in the tomographic retrieval. Moreover, some beams graze a pixel through its corner such that the path lengths of these beams in this pixel are very small and so carry little information about this pixel.

To test the capability of the point-function discretization scheme, two very different cloud cases are selected: a stratocumulus and a patchy cumulus. Both cases are 5 km wide and 1.5 km high snapshots from a large eddy simulation model (Ackerman *et al.* 1995). Four simulated radiometers of 0.3 K noise level and 2-degree beam width are spaced equally along a line of 10 km on the ground. Each radiometer scans the upper plane within 80° elevation of zenith at a 0.35° increment and this scanning strategy results in a total of 900 rays intersecting the 5 km by 1.5 km domain. The brightness temperature data for each ray are computed based on a radiative transfer equation and a prescribed antenna response function (Huang *et al.* 2008a). The point-function discretization scheme described in section 2 is then integrated into a constrained inversion algorithm (Huang *et al.* 2008b) to handle the intertwining issue of ill-posing and discretization.

3.2 *Examination of discretization error and ill-posedness*

The capability of the pixel and point-function discretization schemes to approximate the true images is quantified by the root mean squared (rms) difference between the discretized and original images, whereas the ill-posedness of the retrieval problem is characterized by the condition number of the corresponding kernel matrix **A**, which is the ratio of the maximum to minimum singular values.

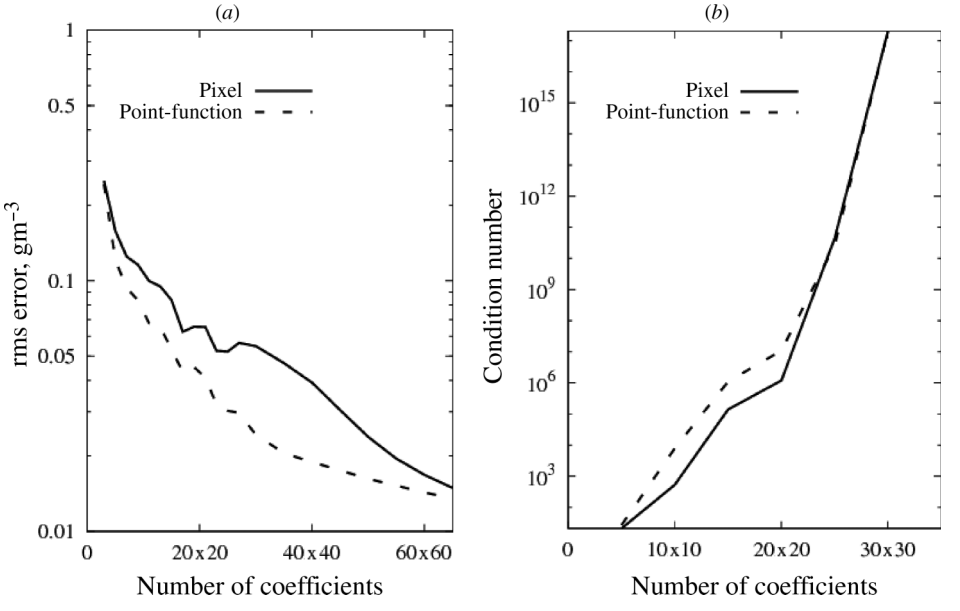

Figure 2. Illustration of the trade-off between discretization error and ill-posedness of the cloud tomography retrieval problem. The discretization errors ((*a*): characterized by rms error) of the pixel and the point-function discretization schemes decrease, but the corresponding condition numbers ((*b*): a measure of ill-posedness) increase, with increasing number of pixels or grid points.

The accuracy of a discretized approximation to a continuous field depends on the smallest scale that the discretization scheme can resolve. This scale is usually determined by the total number of coefficients (pixels or points), n, used in the discretization scheme. With the same number of coefficients, the point-function discretization scheme significantly outperforms the pixel scheme: the rms error of the point-function discretization scheme is about 60–80% of that of the pixel scheme when $25 \leq n \leq 900$; with $n \leq 25$ neither scheme works well while with $n \geq 1600$ both schemes work well (figure 2(*a*)). In contrast, the condition number of the pixel scheme agrees well with that of the point-function scheme in the whole spectrum (figure 2(*b*), high-order singular values would be numerically unstable and thus the condition numbers were not calculated when $n \geq 900$). Note that a larger condition number means a more ill-posed retrieval problem. Furthermore, figure 2 reveals the mixed consequences of using finer discretization: the discretization error unsurprisingly decreases when more pixels or points are used, while the condition number increases with finer discretization. This confirms that discretization error and ill-posedness of the involved retrieval problem trade off against each other and thus using finer discretization may not improve the retrieval.

3.3 *Retrieval results*

The reduction of discretization error by the point-function scheme is expected to improve the retrieval as well. Figure 3 shows the true and retrieved LWC distributions

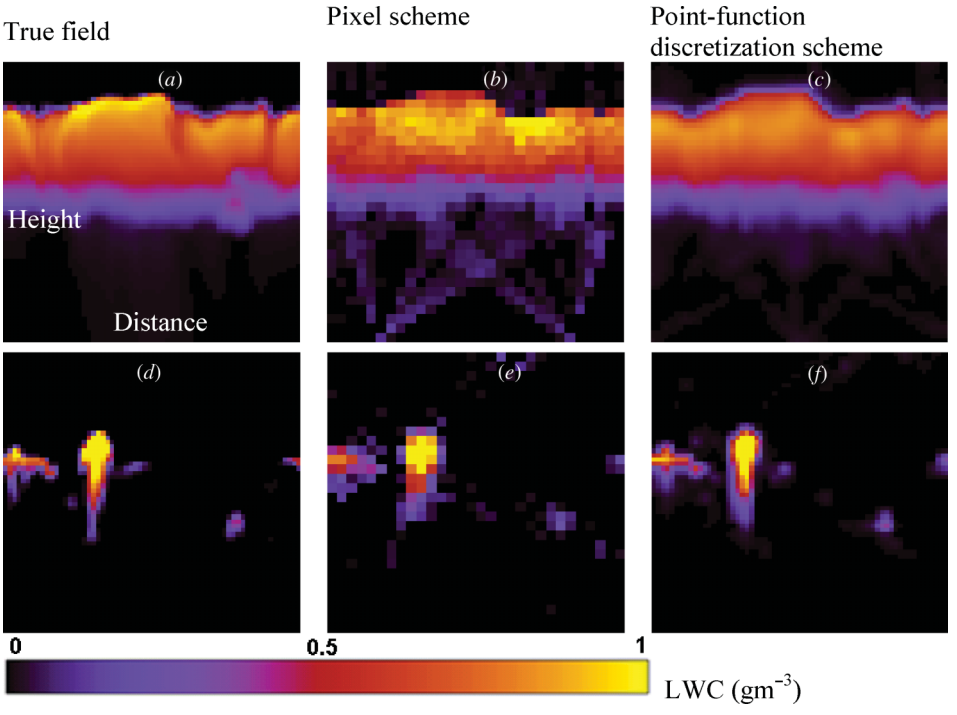

Figure 3. The retrieved images using the pixel and the point-function discretization schemes for two different cloud cases: a stratocumulus case (*a*, *b*, *c*) and a patchy cumulus case (*d*, *e*, *f*). The cloud tomography simulations are based on four radiometers of 0.3 K noise level and 2-degree beam width. For both discretization schemes, $30 \times 30 = 900$ coefficients (pixels or points) are used.

for the two cloud cases obtained by using the pixel and point-function discretization schemes. Although the retrieved images using the pixel scheme reasonably capture the spatial patterns of the original images, they suffer from some noticeable artefacts. For the first cloud case, some spurious clouds appear below the cloud base and over the cloud top (figure 3(*b*)). Furthermore, the scattered clouds below the cloud base are arranged along several lines approximately 20° and 40° off the nadir, which indicates the discretization artefacts. For the broken cumulus cloud case, the retrieved image shows more pieces of clouds compared to the true image (figure 3(*e*)). The shape of the cloud patches is not realistic compared with the true image as well. In contrast, the retrieval using the point-function discretization scheme preserves more features of the original images. The spurious cloud patches disappear in the images retrieved with the point-function discretization scheme for both the stratocumulus and the broken cumulus cases. The geometrical shape of the clouds is also better reproduced with the point-function discretization scheme than that retrieved with the conventional pixel scheme.

For both cloud cases, the retrieval errors corresponding to the point-function discretization scheme are reduced by up to 40% compared to those of the pixel scheme, namely, 0.11 gm^{-3} and 0.069 gm^{-3} for the stratocumulus case, 0.076 gm^{-3} and 0.049 gm^{-3} for the patchy cumulus case.

4. Concluding remarks

A functional discretization scheme, called point-function scheme, has been adopted as a replacement for the conventional pixel scheme. The point-function scheme approximates continuous distributions based on values over a set of points and predefined linear interpolation functions. It is first demonstrated that the point-function discretization scheme yields a significantly smaller discretization error compared to the pixel scheme when the same number of points or pixels are used for each discretization scheme. Then the utility of the new discretization scheme for ill-posed remote sensing problems is illustrated using the example of tomographic retrieval of cloud fields from multi-angular line-integral measurements. The point-function discretization scheme is integrated into a constrained inversion algorithm to handle the interweaving issue of ill-posedness and discretization found in the practice of cloud tomography. This integrated algorithm substantially improves the tomographic retrieval, reducing the retrieval error by up to 40% compared to the conventional pixel scheme.

The point-function discretization scheme indeed has many advantages in applications like tomographic retrieval and atmospheric sounding. With the point-function scheme, the remote sensing retrievals can be re-sampled virtually at any resolution, while with the pixel scheme they can only be coarsened in quantum jumps. This becomes important for synergetic retrieval from dissimilar remote sensing sensors, each sampling at a different resolution, or even worse the resolution difference being range-dependent because of conical beams; in this case, with the point-function representation, one can sample one instrument at the resolution of the other or sample both at a new resolution.

Acknowledgements

This research is supported by the DOE Atmosphere Radiation Measurement program under Contract DE-AC02-98CH10886. We thank Dr. Robert McGraw for insightful discussions on this research.

References

Ackerman, S.A., Toon, O.B. and Hobbs, P.V., 1995, A model for particle microphysics, turbulent mixing, and radiative transfer in the stratocumulus topped marine boundary layer and comparisons with measurements. *Journal of Atmospheric Sciences*, **52**, pp. 1204–1236.

Arfken, G., 1985, *Mathematical Methods for Physicists*, 3rd edition, pp. 1–1209 (Orlando: Academic Press).

Bockmann, C., 2001, Hybrid regularization method for the ill-posed inversion of multiwavelength lidar data in the retrieval of aerosol size distributions. *Applied Optics*, **40**, pp. 1329–1342.

Censor, Y., 1983, Finite series-expansion reconstruction. *Proceedings of the IEEE*, **71**, pp. 409–419.

Delprat-Jannaud, F. and Lailly, P., 1993, Ill-posed and well-posed formulations of the reflection travel time tomography problem. *Journal of Geophysical Research*, **98**, pp. 6589–6605.

Giuli, D., Toccafondi, A., Biffi Gentili, B. and Freni, A., 1991, Tomographic reconstruction of rainfall fields through microwave attenuation measurements. *Journal of Applied Meteorology*, **30**, pp. 1323–1340.

Hansen, P.C., 1998, *Rank Deficient and Ill-Posed Problems: Numerical Aspects of Linear Inversion*, pp. 1–247 (Philadelphia: SIAM).

Huang, D., Liu, Y. and Wiscombe, W., 2008a, Determination of cloud liquid water distribution using 3D cloud tomography. *Journal of Geophysical Research*, **113**, p. D13201, doi:10.1029/2007JD009133.

Huang, D., Liu, Y. and Wiscombe, W., 2008b, Cloud tomography: role of constraints and a new algorithm. *Journal of Geophysical Research*, **113**, p. D23203, doi:10.1029/2008JD009952.

Scales, J.A., Docherty, P. and Gersztenkorn, A., 1990, Regularisation of non-linear inverse problems: imaging the near-surface weathering layer. *Inverse Problems*, **6**, pp. 115–131.

Stephens, G.L., Vane, D.G., Boain, R.J., Mace, G.G., Sassen, K., Wang, Z., Illingworth, A.J., O'connor, E.J., Rossow, W.B., Durden, S.L., Miller, S.D., Austin, R.T., Benedetti, A., Mitrescu, C. and Team, T.C.S., 2002, The CloudSat mission and the A-train. *Bulletin of the American Meteorological Society*, **83**, pp. 1771–1790.

Susskind, J., Barnet, C.D. and Blaisdell, J.M., 2003, Retrieval of atmospheric and surface parameters from AIRS/AMSU/HSB data in the presence of clouds. *IEEE Transactions on Geoscience and Remote Sensing*, **41**, pp. 390–409.

Warner, J., Drake, J.F. and Krehbiel, P.R., 1985, Determination of cloud liquid water distribution by inversion of radiometric data. *Journal of Atmospheric and Oceanic Technology*, **2**, pp. 293–303.